HUTCHINSON-GILFORD PROGERIA

# Splicing-Directed Therapy in a New Mouse Model of Human Accelerated Aging

Fernando G. Osorio,[1] Claire L. Navarro,[2] Juan Cadiñanos,[1]* Isabel C. López-Mejía,[3] Pedro M. Quirós,[1] Catherine Bartoli,[2] José Rivera,[4] Jamal Tazi,[3] Gabriela Guzmán,[5] Ignacio Varela,[1] Danielle Depetris,[2] Félix de Carlos,[6] Juan Cobo,[6] Vicente Andrés,[4] Annachiara De Sandre-Giovannoli,[2,7] José M. P. Freije,[1] Nicolas Lévy,[2,7] Carlos López-Otín[1†]

**Hutchinson-Gilford progeria syndrome (HGPS) is caused by a point mutation in the *LMNA* gene that activates a cryptic donor splice site and yields a truncated form of prelamin A called progerin. Small amounts of progerin are also produced during normal aging. Studies with mouse models of HGPS have allowed the recent development of the first therapeutic approaches for this disease. However, none of these earlier works have addressed the aberrant and pathogenic *LMNA* splicing observed in HGPS patients because of the lack of an appropriate mouse model. Here, we report a genetically modified mouse strain that carries the HGPS mutation. These mice accumulate progerin, present histological and transcriptional alterations characteristic of progeroid models, and phenocopy the main clinical manifestations of human HGPS, including shortened life span and bone and cardiovascular aberrations. Using this animal model, we have developed an antisense morpholino–based therapy that prevents the pathogenic *Lmna* splicing, markedly reducing the accumulation of progerin and its associated nuclear defects. Treatment of mutant mice with these morpholinos led to a marked amelioration of their progeroid phenotype and substantially extended their life span, supporting the effectiveness of antisense oligonucleotide–based therapies for treating human diseases of accelerated aging.**

## INTRODUCTION

Progeroid laminopathies, including Hutchinson-Gilford progeria syndrome (HGPS), are human disorders of accelerated aging caused by defects in nuclear A–type lamins. The HGPS clinical phenotype is characterized by growth impairment, lipodystrophy (fat redistribution), dermal and bone abnormalities, and cardiovascular alterations, leading to shortened life span (*1*, *2*). Most HGPS patients carry a heterozygous point mutation within exon 11 of the *LMNA* gene encoding lamin A [a C-to-T transition in the *LMNA* coding region at nucleotide 1824 (c.1824C>T); no putative change in the protein sequence, because both encode a glycine at amino acid position 608 (p.Gly608Gly)] (*3*, *4*). Lamin A is a core component of the nuclear envelope that undergoes a complex maturation process, including the addition of a farnesyl group and a proteolytic processing event carried out by the metalloprotease ZMPSTE24/FACE1. The p.Gly608Gly mutation activates a cryptic splicing donor site that leads to the accumulation of a truncated form of prelamin A, called LAΔ50 or progerin, which has an internal deletion of 50 amino acids encompassing the target sequence for cleavage by ZMPSTE24. The accumulation of farnesylated progerin at the nuclear envelope leads to the functional and structural defects observed in the nucleus of affected patients (*5*, *6*). Progerin is not only detected in HGPS patients but also during normal aging, thereby adding a new level of interest to the study of the mechanisms that underlie progerin formation and accumulation in human cells and tissues (*7*, *8*).

Over the past few years, several mouse models of progeroid laminopathies have been generated (*9*–*14*), providing valuable information about the molecular alterations functionally involved in these diseases (*15*–*18*) and allowing the development of strategies to test anti-progeria therapeutic approaches (*19*–*22*). Although some of these models, especially *Zmpste24*-deficient mice (*9*, *10*), phenocopy most alterations present in HGPS, none of them reproduce the molecular situation that occurs at the *LMNA* locus of these patients. These differences have represented a serious limitation for both the study of splicing alterations in HGPS and the development of in vivo treatments with drugs that specifically modify *LMNA* splicing (*23*). Here, we describe the generation and characterization of a mouse model that carries the precise HGPS mutation. With this new model, we were able to test in vivo therapies aimed at targeting the abnormal *LMNA* splicing that occurs in both normal and pathological aging.

## RESULTS

To generate a knock-in mouse strain carrying the HGPS mutation, we designed a strategy for replacement of the wild-type mouse *Lmna* gene with a mutant allele that carried the c.1827C>T;p.Gly609Gly mutation, which is equivalent to the HGPS c.1824C>T;p.Gly608Gly mutation in the human *LMNA* gene (Fig. 1A). In an attempt to avoid the breeding problems present in other mouse models that express progerin (*19*), we designed a conditional mutant allele with a *neomycin resistance* gene flanked by two loxP sites inserted in *Lmna* intron 10. This cassette was able to prevent the formation of prelamin A transcripts

[1]Departamento de Bioquímica y Biología Molecular, Facultad de Medicina, Instituto Universitario de Oncología, Universidad de Oviedo, 33006 Oviedo, Spain. [2]Université de la Méditerranée, Inserm UMR_S 910, Faculté de Médecine de Marseille, 13385 Marseille cedex 05, France. [3]Institut de Génétique Moléculaire, UMR 5535 CNRS, 34293 Montpellier cedex 5, France. [4]Departamento de Epidemiología, Aterotrombosis e Imagen, Centro Nacional de Investigaciones Cardiovasculares, 28029 Madrid, Spain. [5]Servicio de Cardiología, Hospital Universitario La Paz, 28046 Madrid, Spain. [6]Departamento de Cirugía y Especialidades Médico-Quirúrgicas and Instituto Asturiano de Odontología, Universidad de Oviedo, 33006 Oviedo, Spain. [7]AP-HM, Département de Génétique Médicale, Hôpital d'Enfants de la Timone, 13385 Marseille cedex 05, France.
*Present address: Instituto de Medicina Oncológica y Molecular de Asturias, Centro Médico de Asturias, 33193 Oviedo, Spain.
†To whom correspondence should be addressed. E-mail: clo@uniovi.es

by blocking lamin A–specific splicing. Therefore, this allele, which we refer to as *Lmna*$^{LCS}$ (Lamin C–Stop), directs only the expression of lamin C and allows study of the potential effects of lamin A deficiency (Fig. 1A). We generated *Lmna*$^{LCS/+}$ mice and crossed them with a *Cre*-deleter mouse strain to obtain germline removal of the *neomycin resistance* cassette (Fig. 1, A and B). As a result, we obtained offspring that carried the *Lmna*$^{G609G}$ knock-in allele, which expressed lamin C, lamin A, and progerin (Fig. 1C).

To ensure the correct translation of the mutant allele, we analyzed protein extracts from cultures of mouse fibroblasts of each genotype by Western (immuno) blot with a specific antibody that recognizes lamin A/C (Fig. 1C). Genomic analysis of *Lmna* exon 11 confirmed the genotypes of *Lmna*$^{+/+}$, *Lmna*$^{G609G/+}$, and *Lmna*$^{G609G/G609G}$ mice (fig. S1). Likewise, semiquantitative transcriptional analysis and direct sequencing of RNA samples from several tissues confirmed that the aberrant *Lmna* splicing in *Lmna*$^{G609G}$ mice was equivalent to the *LMNA* splicing error that occurs in HGPS patients (*3*, *4*) (fig. S1). Finally, several tissue samples from *Lmna*$^{+/+}$, *Lmna*$^{G609G/+}$, and *Lmna*$^{G609G/G609G}$ mice were analyzed further by Western blotting, which confirmed the expected lamin A/C and progerin expression patterns (fig. S2).

Homozygous mice for the conditional *Lmna*$^{LCS}$ allele were indistinguishable from their wild-type littermates and did not show any detectable differences in growth or longevity up to 50 weeks of age (fig. S3), which is in agreement with previous reports on the dispensability of the lamin A isoform (*24*). Conversely, mice that carried the *Lmna*$^{G609G}$ allele expressed lamin C, lamin A, and progerin, reproducing the same molecular situation as is present in HGPS patients. Homozygous mice with the c.1827C>T;p.Gly609Gly mutation were infertile but seemed healthy until 3 weeks of age. Subsequently, they showed a reduction in growth rates (Fig. 2A), with a progressive loss of weight (Fig. 2B) and the acquisition of an abnormal posture and a marked curvature of the spine (cervicothoracic lordokyphosis) (Fig. 2D). These multiple alterations finally resulted in premature death of these mutant mice, which have an average life span of 103 days (Fig. 2C) compared to more than 2 years for wild-type mice. Heterozygous *Lmna*$^{G609G/+}$ mice had normal weight, size, and fertility until about 8 months of age. At that point, the mice started to lose weight, exhibiting a process similar to that observed in homozygous mice and causing their premature death at an average of 242 days. Both heterozygous and homozygous mice that carried the c.1827C>T;p.Gly609Gly mutation showed profound nuclear abnormalities as a consequence of progerin accumulation (Fig. 2E).

As a starting point for phenotypic characterization of mice that carried the c.1827C>T;p.Gly609Gly mutation, we focused on *Lmna*$^{G609G/G609G}$ mice, which show a more pronounced and earlier progeroid phenotype than heterozygous *Lmna*$^{G609G/+}$ mice. The relatively milder phenotype of *Lmna*$^{G609G/+}$ mice, compared with *LMNA*$^{G608G/+}$ HGPS patients, is in agreement with previous observations that have evidenced a higher tolerance of mice compared to humans when it comes to accumulation of prelamin A forms. Thus, the complete absence of prelamin A processing as a result of full *ZMPSTE24* deficiency causes reduced fetal weight, premature delivery, and perinatal death in humans, whereas the same molecular alteration produces no overtly detectable phenotype in mice until 3 to 4 weeks after birth (*9*, *25*). Accordingly, homozygous *Lmna*$^{G609G/G609G}$ mice likely are a better model of HGPS than are *Lmna*$^{G609G/+}$ heterozygotes.

*Lmna*$^{G609G/G609G}$ mice of advanced age exhibited a generalized loss of the principal fat deposits. Microscopy analysis of the skin revealed loss of the subcutaneous fat layer and a general attrition of hair follicles (Fig. 2F). Senescence-associated β-galactosidase staining was increased in liver and kidney sections from 3-month-old *Lmna*$^{G609G/G609G}$ mice when compared with age-matched wild-type animals (Fig. 2F), reflecting a premature aging process in these animals.

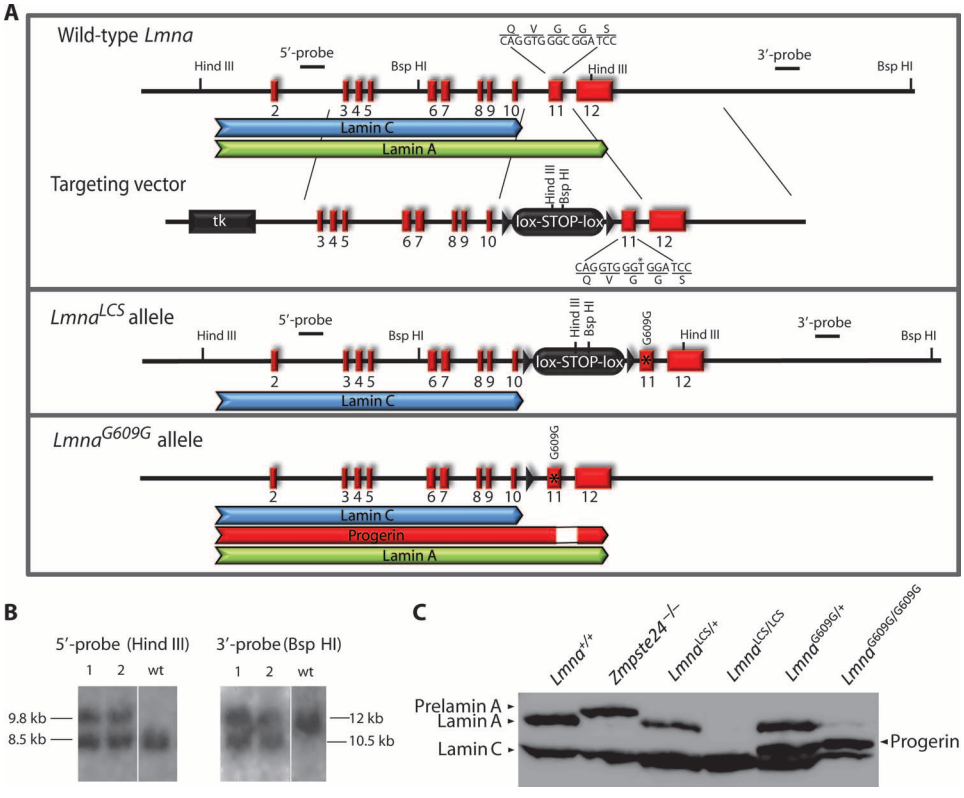


**Fig. 1.** Generation of knock-in *Lmna*$^{G609G}$ mice. (**A**) Schematic representation of the wild-type *Lmna* locus, targeting vector, and targeted allele. Positions of restriction enzyme cleavage sites and probes used for Southern blot analysis are shown. (**B**) Southern (DNA) blot analysis of genomic DNA from two targeted *Lmna*$^{LCS}$-ES cell clones and wild-type ES. Probing of Hind III–digested DNA revealed fragments of 9.8 and 8.5 kb for mutant and wild-type (wt) alleles, respectively. Probing of Bsp HI–digested DNA revealed fragments of 12 and 10.5 kb for wt and mutant alleles, respectively. (**C**) Western (immuno) blot analysis of mouse adult fibroblasts obtained from the mice with the various genotypes used in the study. Lamin A, lamin C, prelamin A, and progerin were detected with a monoclonal antibody against lamin A/C (Manlac-1).

The size of most organs from homozygous mutant mice was proportional to their reduced body weight (fig. S4), but the main lymphoid organs, thymus and spleen, exhibited a marked involution relative to wild-type animals (Fig. 2F). Similar alterations are shown by other progeroid mouse models in association with defects in the immune system (*26*, *27*). Microcomputed tomography (μCT) analysis of tibias, skull, and vertebral column revealed profound bone alterations in $Lmna^{G609G/G609G}$ mice compared to wild-type mice. Thus, the tibias of mutant mice showed a reduction in bone density and cortical thickness as well as an increased porosity (Fig. 3A). Likewise, skulls showed a clear size reduction and smaller lower incisors, whereas vertebral column analysis confirmed a marked lordokyphosis in homozygous mutant mice (fig. S5, A and B). $Lmna^{G609G/G609G}$ mice also showed reduced grip strength (fig. S5C).

Moreover, mutant mice exhibited important cardiovascular alterations that could be related to their premature death and that also occur in HGPS patients as well as during normal aging (*28*). Because vascular smooth muscle cell (VSMC) depletion has been reported in another progeroid mouse model (*12*) and in some HGPS patients (*29*), we focused on the study of these cells. The number of VSMCs in the medial layer of the thoracic aorta was similar in wild-type and $Lmna^{G609G/G609G}$ mice (fig. S6A), but $Lmna^{G609G/G609G}$ mice displayed a significant loss of VSMCs in the aortic arch, a region that exhibits extensive branching and is subjected to high hemodynamic stress (Fig. 3B). Notably, the severity of this phenotype in one HGPS patient correlated with hemodynamic stress around the site of branching (*29*). Blood pressure appeared normal in $Lmna^{G609G/G609G}$ mutant mice (fig. S6B), but they progressively developed bradycardia between 9 and 15 weeks of age (Fig. 3B). Moreover, electrocardiographic (ECG) studies revealed prolonged QRS waves in $Lmna^{G609G/G609G}$ mice without changes in the PR interval (Fig. 3B) relative to wild-type mice, which indicates an alteration of heart ventricular depolarization. Finally, we assessed heart function by transthoracic echocardiography. Both M-mode and Simpson's method two-dimensional (2D) echocardiography of left ventricular function revealed no differences in systolic function (ejection fraction and fractional shortening) or diastolic

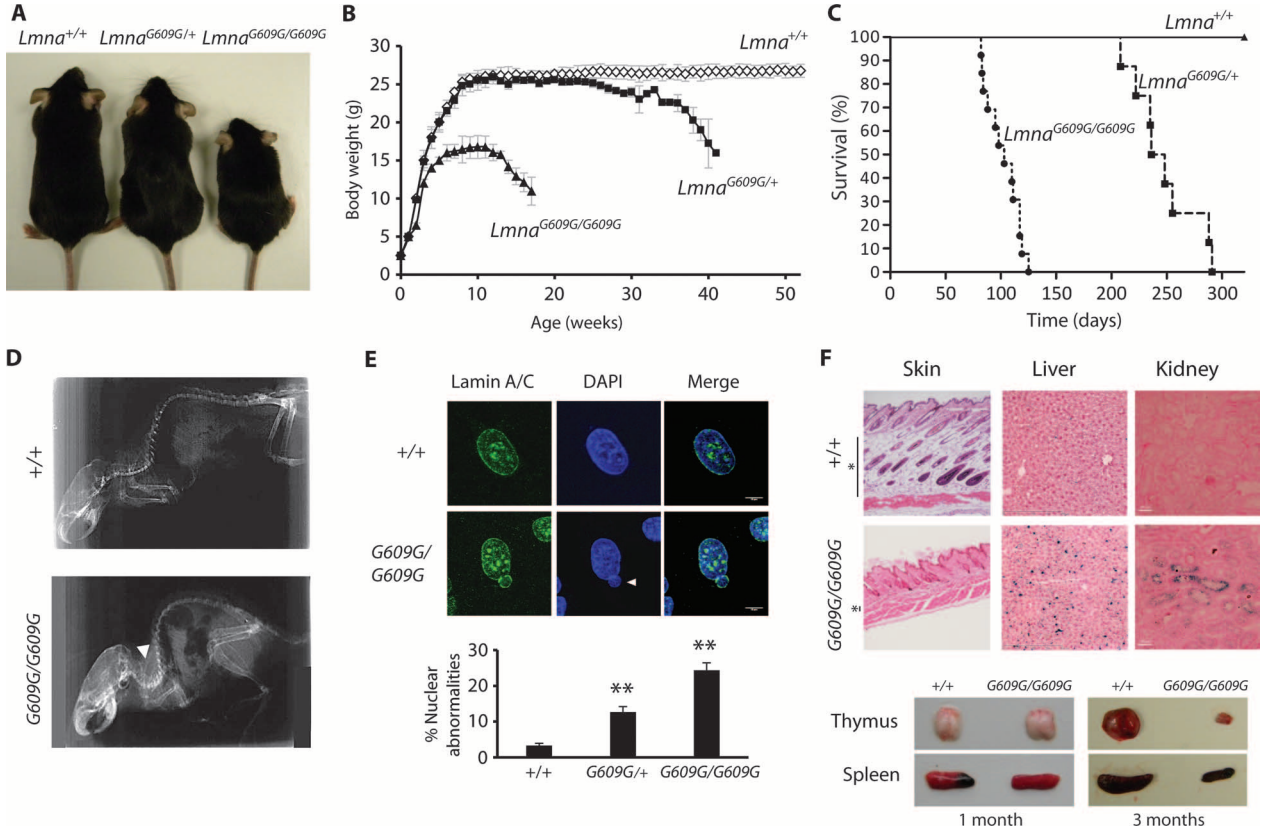


**Fig. 2.** Phenotypes of $Lmna^{G609G}$ mice. (**A**) Representative photographs of 3-month-old $Lmna^{+/+}$, $Lmna^{G609G/+}$, and $Lmna^{G609G/G609G}$ mice. (**B**) Cumulative plot of body weight versus age. Dots represent mean values, and error bars indicate SDs ($n > 10$ for each genotype) ($P < 0.01$ for all the comparisons, ANOVA test). (**C**) Kaplan-Meier survival plots for $Lmna^{G609G/G609G}$ ($n = 12$), $Lmna^{G609G/+}$ ($n = 8$), and $Lmna^{+/+}$ mice ($n = 15$) [$P < 0.01$ for all the comparisons, log-rank (Mantel-Cox) test]. (**D**) Radiograph of a 3-month-old $Lmna^{G609G/G609G}$ mouse compared with a wild-type littermate. (**E**) Nuclear envelope architecture analyzed in $Lmna^{G609G/G609G}$ and $Lmna^{+/+}$ fibroblasts with an anti–lamin A/C antibody and counterstained with DAPI (top panel). The white arrowhead indicates a representative example of membrane blebbing in an abnormal nucleus. The plot reflects the percentage of nuclei with abnormalities (nuclei with blebbing or irregular shape) in $Lmna^{+/+}$, $Lmna^{G609G/+}$, and $Lmna^{G609G/G609G}$ fibroblast cell lines. Error bars represent SDs. $^{**}P < 0.01$ (two-tailed Student's $t$ test) compared to control (+/+) values (bottom panel). (**F**) H&E staining of skin from a 3-month-old $Lmna^{G609G/G609G}$ mouse compared with that of a wild-type littermate (asterisks indicate subcutaneous fat layer). Senescence-associated β-galactosidase activity in sections of liver and kidney from $Lmna^{G609G/G609G}$ and wild-type littermate (top panel). Representative photographs of thymus and spleen from $Lmna^{G609G/G609G}$ and wild-type littermates at 1 and 3 months of age (bottom panel).

function (mitral valve inflow velocity E to A ratio) in *Lmna*$^{G609G/G609G}$ mutant versus wild-type mice (fig. S6C).

*Lmna*$^{G609G/G609G}$ mice also showed, relative to wild-type mice, altered circulating plasma concentrations of various hormones and other biochemical markers. For example, at 2 months of age, the *Lmna*$^{G609G/G609G}$ mutant mice showed a decrease in serum glucose concentrations, relative to wild-type mice, an alteration that worsened with age, leading to extreme hypoglycemia at 3 months of age (Fig. 3C). We also observed a decrease of serum glucose concentrations in heterozygous *Lmna*$^{G609G/+}$ mutant mice of advanced age (8 months), indicating

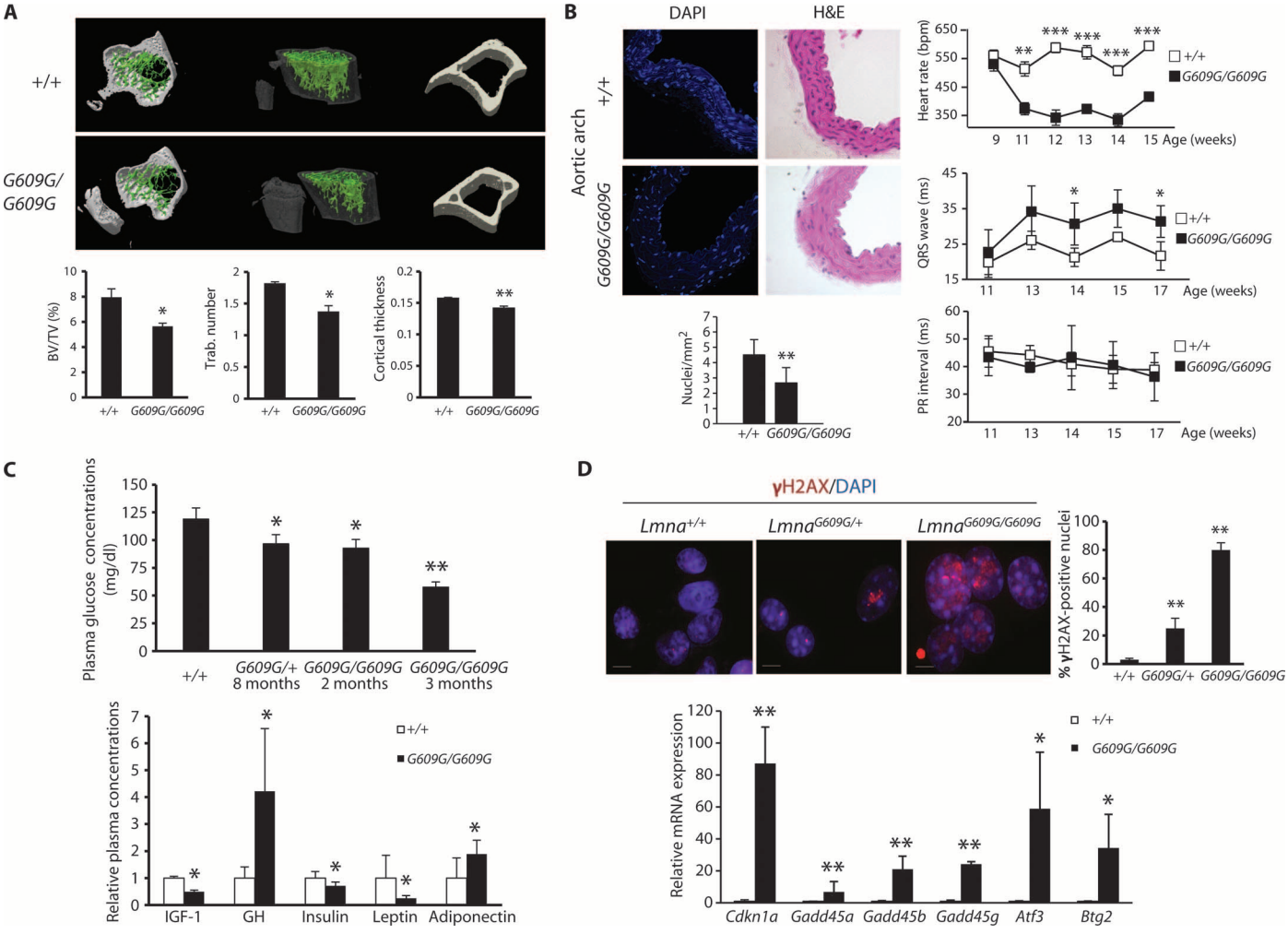


**Fig. 3.** Bone, cardiovascular, and biochemical alterations in *Lmna*$^{G609G/G609G}$ mice. (**A**) 3D image generated from μCT analysis of tibias from 3-month-old *Lmna*$^{G609G/G609G}$ and *Lmna*$^{+/+}$ mice (top panel). Bottom panel contains quantitative analysis of relative bone volumes [bone volume/tissue volume (BV/TV)], number of trabecules per millimeter, and cortical thickness in *Lmna*$^{G609G/G609G}$ ($n = 4$) and *Lmna*$^{+/+}$ ($n = 4$) mice. Mean values are represented, and error bars indicate SDs. *$P < 0.05$; **$P < 0.01$ (two-tailed Student's $t$ test) compared to control (+/+) values. (**B**) Representative photographs showing VSMC depletion in the medial layer of the aortic arch (top left panel). Cross sections were stained with DAPI and H&E. Plot represents the average from 14 to 17 independent cross sections (bottom left panel). Right panels show the results of longitudinal studies to assess heart rate and ECG parameters ($n = 4$). Heart rate is represented as the number of beats per minute (bpm). Mean values are represented and error bars indicate SDs. *$P < 0.05$; **$P < 0.01$; ***$P < 0.001$ (two-tailed Student's $t$ test) compared to control (+/+) values. (**C**) Blood glucose concentrations in *Lmna*$^{+/+}$ ($n = 5$), 8-month-old *Lmna*$^{G609G/+}$ ($n = 4$), and 2- ($n = 6$) and 3-month-old ($n = 6$) *Lmna*$^{G609G/G609G}$ mice, respectively (top panel). Mean values are represented and error bars indicate SDs. *$P < 0.05$; **$P < 0.01$ (two-tailed Student's $t$ test) compared to control (+/+) values. Bottom panel shows comparisons of plasma concentrations of IGF-1, GH, insulin, leptin, and adiponectin between *Lmna*$^{G609G/G609G}$ ($n = 4$) and wild-type littermates ($n = 4$). Concentrations were normalized to the mean of control (+/+). Error bars indicate SDs. *$P < 0.05$ (two-tailed Student's $t$ test) compared to control (+/+) values. (**D**) Indirect immunofluorescence staining of γH2AX in P5 skin fibroblasts issued from *Lmna*$^{+/+}$, *Lmna*$^{G609G/+}$, and *Lmna*$^{G609G/G609G}$ mice (top left panel). The number of enlarged nuclei that showed γH2AX foci staining for each cell line is reported on the graph. Three independent experiments were performed for each genotype. $F = 4.05$ ($F$, found variation of the group averages/expected variation of the group averages); mean values are represented and error bars indicate SDs. **$P < 0.005$ (ANOVA) compared to control (+/+) values. Contribution of the genotype to the variance: 32% (Cohen's $d$ Ryan test) (top right panel). Transcriptional analysis by real-time quantitative PCR of p53 targets in 3-month-old *Lmna*$^{G609G/G609G}$ and *Lmna*$^{+/+}$ mice (bottom panel). mRNA levels were normalized to the mean of *Lmna*$^{+/+}$ liver mRNA. Error bars represent SDs. *$P < 0.05$; **$P < 0.01$; ***$P < 0.001$ (two-tailed Student's $t$ test) compared to control (+/+) values.

that hypoglycemia might also contribute to the cardiovascular compromise and early death of mice that carried the c.1827C>T;p.Gly609Gly mutation. In addition, $Lmna^{G609G/G609G}$ mice showed decreased serum levels of insulin-like growth factor 1 (IGF-1), insulin, and leptin and increased levels of growth hormone (GH) and adiponectin relative to wild-type mice (Fig. 3C).

As a measure of genotoxic stress, we analyzed histone γH2AX levels—a marker for the amount of nuclear DNA double-strand breaks—in the nuclei of cultured fibroblasts from mice of the various genotypes (Fig. 3D). Most (81%) $Lmna^{G609G/G609G}$ fibroblasts at passage 5 (P5) contained large and abnormally shaped nuclei with foci that were highly stained with anti-γH2AX antibodies. Similar abnormal nuclei were identified in 24% of $Lmna^{G609G/+}$ fibroblasts and in 3% of $Lmna^{+/+}$ fibroblasts (Fig. 3D).

To elucidate the molecular pathways that underlie the phenotypic alterations described in $Lmna^{G609G/G609G}$ mice, we analyzed the transcription profiles of livers from $Lmna^{G609G/G609G}$ mutant mice and wild-type littermates using complementary DNA (cDNA) hybridization to DNA microarrays. A large number of genes showed reproducible changes in their expression levels in the mutant mice, consistent with the critical roles of nuclear lamins in chromatin structure and function (*30*) (table S1). From these data, gene set enrichment analysis (GSEA) was used for an unbiased identification of molecular pathways that were significantly altered in these mice (*31*). This analysis revealed a very strong correlation between the transcriptional alterations detected in these $Lmna^{G609G/G609G}$ and *Zmpste24*-deficient mice (*32*), supporting the existence of a common transcriptional signature in two different models of progeroid laminopathies.

Functionally, most of the pathways that were significantly enriched in $Lmna^{G609G/G609G}$ samples are associated with stress responses. Thus, the p53 tumor suppressor pathway (Fig. 3D) and the ATM (ataxia telangiectasia mutated)–related pathway are significantly up-regulated in $Lmna^{G609G/G609G}$ mice, probably as a consequence of unrepaired DNA damage caused by progerin accumulation (*33*). We previously hypothesized that these alterations, including chronic activation of the p53 pathway, are drivers of the senescent phenotype displayed by these mice (*32*). Moreover, the list of genes that were overexpressed in the $Lmna^{G609G/G609G}$ mutant mice relative to wild-type animals contains a significant number of components of the hypoxia response pathway mediated by induction of the HIF-1α (hypoxia-inducible factor 1α) transcription factor (fig. S7). This pathway recently was associated with metabolic changes in a mouse model of progeria and could be involved in the serum glucose alterations seen in these mice (*34*). Other pathways that were down-regulated in $Lmna^{G609G/G609G}$ mice are related to metabolic processes such as fatty acid metabolism, oxidative phosphorylation, and mitochondria biogenesis (figs. S7 and S8).

The marked similarities in the molecular alterations observed in $Lmna^{G609G}$ mice and HGPS patients prompted us to develop an in vivo therapeutic approach based on the use of morpholino antisense oligonucleotides (*35*). Morpholinos are small modified oligonucleotides that can block splicing events by preventing access of the splicing machinery to the splice sites (*36*). In contrast with other unmodified oligonucleotides, morpholinos are stable and do not induce ribonuclease (RNase) H–driven degradation of the morpholino-RNA heteroduplex. Previous in vitro studies have demonstrated how a 25-nucleotide morpholino that specifically binds the human c.1824C>T;p.Gly608Gly HGPS mutation in the altered *LMNA* transcript can restore normal *LMNA* splicing in fibroblasts from HGPS patients, correcting the main pathological alterations of these cells, including nuclear abnormalities and mislocalization of other nuclear envelope proteins (*23*). The lack of phenotypic alterations in mice homozygous for the $Lmna^{LCS}$ allele (fig. S3) prompted us to design a new approach based on modulation of *Lmna* splicing through interfering with the lamin A–specific splice donor site.

Thus, we designed a 25-nucleotide morpholino (MmEx10) that bound to the exon 10–lamin A splice donor site (Fig. 4A). In addition, using the same coordinates as were specified in the original human HGPS targeting experiments (*23*), we designed another 25-nucleotide morpholino that bound the c.1827C>T;p.Gly609Gly mutated sequence in the region of the *Lmna* transcript that corresponded to exon 11 (MmEx11), to test whether the combined administration of both morpholinos could be more effective at reducing progerin amounts than the separate administration of each individual oligonucleotide. In an initial attempt to evaluate the effects of these morpholinos on splicing of the $Lmna^{G609G}$ allele, we transfected the oligonucleotide reagents into a fibroblast cell line derived from a heterozygous mouse that carried the c.1827C>T;p.Gly609Gly mutation and found that both MmEx10 and MmEx11 morpholinos each reduced progerin amounts in a dose-dependent manner; MmEx10 was more effective than MmEx11 at reducing progerin concentrations when the morpholinos were administered separately (30% reduction in 10 μM MmEx11–treated cells when compared to untreated cells; 40% reduction in 10 μM MmEx10–treated cells when compared to untreated cells; $P < 0.01$). When the two reagents were administered to cells at the same time (at a final concentration of 40 μM), progerin amounts were reduced to undetectable levels (Fig. 4B). We obtained similar results after using the human equivalents of the morpholinos in an HGPS fibroblast cell line (Fig. 4B). We also observed that progerin reduction mediated by administration of morpholinos correlated with the correction of nuclear abnormalities in a cell line carrying the homozygous c.1827C>T;p.Gly609Gly mutation and in an HGPS fibroblast cell line (fig. S9). Thus, both independent administration of each morpholino and their combined administration were able to reduce, in a dose-dependent manner, the percentage of cells with nuclear abnormalities to wild-type levels (Fig. 4C).

On the basis of these in vitro studies, we next explored the effect of these antisense oligonucleotides on the progeroid phenotype of $Lmna^{G609G/G609G}$ mice. To this end, we chose a vivo-morpholino delivery approach. Vivo-morpholinos consist of a morpholino oligonucleotide with a covalent link to an octa-guanidine dendrimer that facilitates efficient delivery into most mouse tissues (*37*). To attempt to obtain a maximum in vivo reduction of progerin concentrations, we treated mice either with a control vivo-morpholino or with a combination of MmEx10-MmEx11 vivo-morpholinos. Mutant mice treated with MmEx10-11 showed significantly improved body weights, reduced degrees of lordokyphosis, and extended life spans (Fig. 4D). Thus, the mean survival of treated $Lmna^{G609G/G609G}$ mice was extended from 111 to 155 days, and the maximum survival from 119 to 190 days ($P < 0.001$; Fig. 4D). No significant differences were recorded in survival or body weight between untreated and control vivo-morpholino–treated $Lmna^{G609G/G609G}$ mice (Fig. 4D). To assess the direct effect of morpholino treatment, we carried out reverse transcription–polymerase chain reaction (RT-PCR) experiments and Western blot analyses on mice tissues, which demonstrated clear reductions in progerin mRNA and protein concentrations, respectively, in all tissues analyzed except

skeletal muscle, in which we could detect only a slight reduction in progerin concentrations (Fig. 4E and figs. S10 and S11).

To evaluate the biological effect of morpholino treatment in the reversion of the phenotypical alterations displayed by *Lmna*$^{G609G/G609G}$ mice, we analyzed the abundance of several p53 targets in treated mice as a marker of the senescent phenotype, and remarkably found a more than fivefold reduction in *Cdkn1a*, *Gadd45g*, and *Atf3* mRNA levels in the liver of MmEx10-11–treated *Lmna*$^{G609G/G609G}$ mice in comparison with *Lmna*$^{G609G/G609G}$-untreated mice (fig. S12A). MmEx10-11–treated mice also showed significantly increased serum glucose concentrations compared with untreated *Lmna*$^{G609G/G609G}$ mice ($P < 0.01$, two-tailed Student's $t$ test) (fig. S12B), a thicker subcutaneous fat layer, and reduced staining for senescence-associated β-galactosidase activity in kidney. Treated *Lmna*$^{G609G/G609G}$ mice also showed a reduced involution of thymus and spleen compared with untreated *Lmna*$^{G609G/G609G}$ mice (fig. S12C).

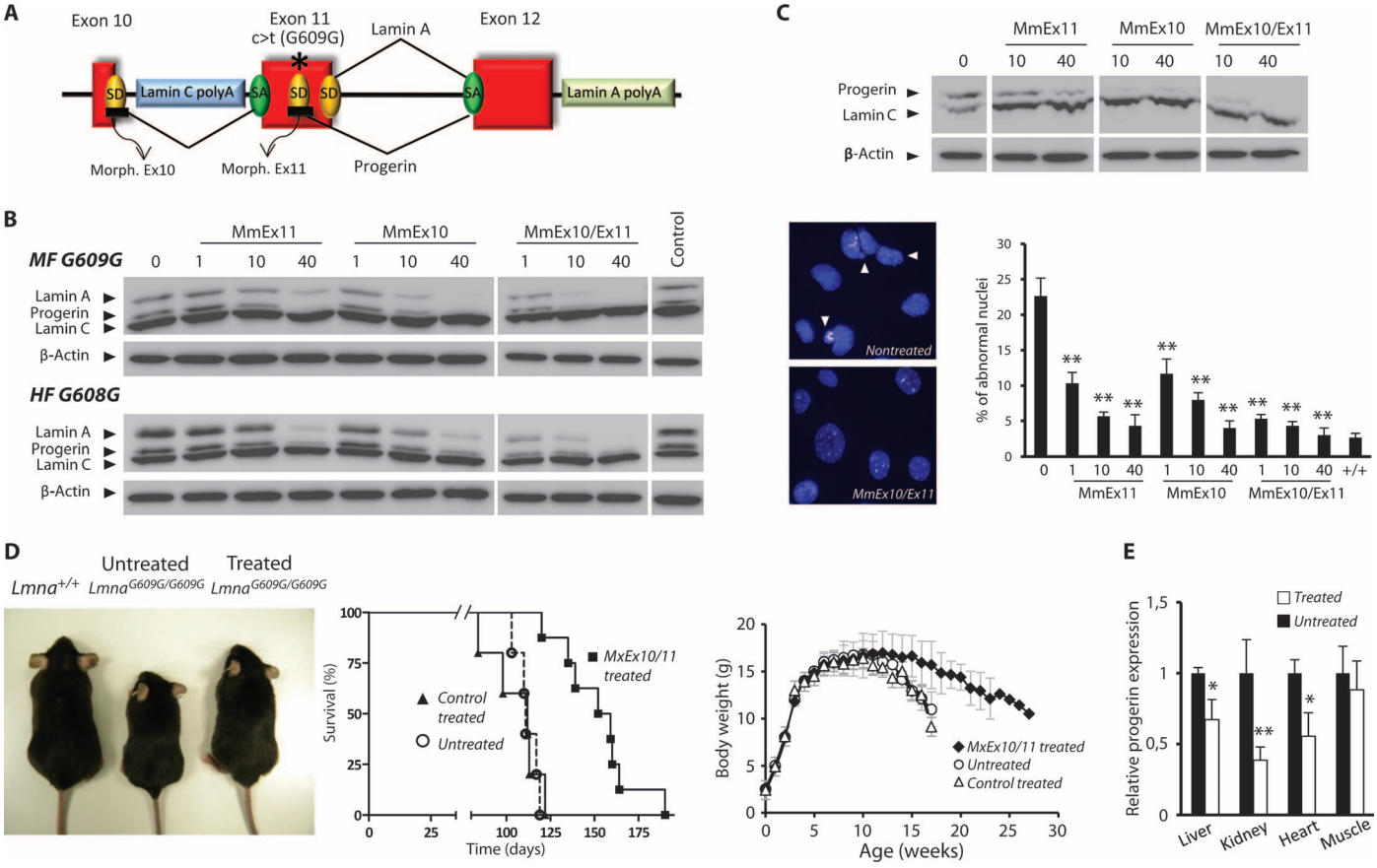


**Fig. 4.** Prevention of progeroid phenotypes upon treatment with antisense morpholino oligonucleotides. (**A**) Schematic representation of the morpholino-based strategy for *Lmna* splicing modulation. (**B**) Western (immuno) blot analysis of mouse *G609G/+* fibroblasts (MF) treated with varying concentrations of morpholinos MmEx10 and MmEx11 (top panel). AG01972c HGPS fibroblasts (HF) treated with varying concentrations of morpholinos HsEx10 and HsEx11 (bottom panel). Lamin A, lamin C, and progerin were detected with a monoclonal antibody against lamin A/C (Manlac-1). β-Actin was used as a loading control. As a specificity control, human morpholinos were used in mouse cells and mouse morpholinos were used in human cells at their maximum concentrations. (**C**) Nuclear envelope architecture analyzed in an *Lmna*$^{G609G/G609G}$ fibroblast cell line treated with varying concentrations (μM) of MmEx10 and MmEx11 morpholinos. Top panel shows Western blot analysis of lamin A/C in morpholino-treated cells. Bottom panel shows a quantitative analysis of nuclear abnormalities (right) and a representative photograph (left) of *Lmna*$^{G609G/G609G}$-untreated and morpholino-treated cells. White arrowheads indicate representative examples of abnormal nuclei. For each morpholino concentration, 300 nuclei were analyzed. Mean values are represented and error bars indicate SDs. $^{**}P < 0.01$ (two-tailed Student's $t$ test) compared to values of untreated cells. (**D**) Representative photograph of a 3-month-old *Lmna*$^{+/+}$ mouse, a *Lmna*$^{G609G/G609G}$ mouse, and a *Lmna*$^{G609G/G609G}$ mouse treated with a combination of MmEx10-MmEx11 (6 mg/kg per day) (left panel). Kaplan-Meier survival plot (middle-left panel) showing a significant increase in life span in MmEx10-MmEx11–treated ($n = 8$) compared with untreated ($n = 5$) and control vivo-morpholino–treated *Lmna*$^{G609G/G609G}$ mice ($n = 5$) ($P < 0.01$ for the comparison between MmEx10-MmEx11–treated and nontreated *Lmna*$^{G609G/G609G}$ mice; $P < 0.01$ for the comparison between MmEx10-MmEx11 and control-treated *Lmna*$^{G609G/G609G}$ mice; log-rank/Mantel-Cox test). Middle-right panel shows a body weight versus age plot of untreated, control vivo-morpholino–treated, and MmEx10-MmEx11 vivo-morpholino–treated *Lmna*$^{G609G/G609G}$ mice. Mean values are represented and error bars indicate SDs ($P < 0.01$ for the comparison between MmEx10-MmEx11–treated and untreated *Lmna*$^{G609G/G609G}$ mice; $P < 0.01$ for the comparison between MmEx10-MmEx11–treated and control-treated *Lmna*$^{G609G/G609G}$ mice; ANOVA test). (**E**) qRT-PCR analysis of progerin mRNA in various tissues from MmEx10-11 vivo-morpholino–treated ($n = 3$) and untreated *Lmna*$^{G609G/G609G}$ ($n = 3$) mice. mRNA levels were normalized to the mean of untreated animals. Error bars indicate SDs. $^{*}P < 0.05$; $^{**}P < 0.01$ (two-tailed Student's $t$ test).

## DISCUSSION

We have previously provided preclinical proof of principle that the combined use of statins (pravastatin) and aminobisphosphonates (zoledronate) could ameliorate several HGPS parameters, including growth, bone density, and survival, by reducing progerin prenylation (*20*). On the basis of these findings, together with additional work from other groups (*19*), two clinical trials were designed and are ongoing in children affected with HGPS (ClinicalTrials.gov #NCT00731016 and #NCT00916747). These therapeutic approaches are aimed at reducing progerin toxicity by pharmacologically inhibiting its prenylation, whereas the one we propose in this study aims to lower the intracellular quantities of the mutant protein itself. The preclinical in vivo success of this approach in the $Lmna^{G609G}$ knock-in mouse model, which most closely mimics the genetics and pathophysiology of HGPS in patients, represents a fundamental proof of concept in the field of progeria therapeutics.

We have shown that $Lmna^{G609G}$ knock-in mice constitute a valuable model for the study of human accelerated aging syndromes because they recapitulate most of the described alterations associated with HGPS. The accumulation of progerin in $Lmna^{G609G/G609G}$ tissues is responsible for a progeroid syndrome characterized by a shortened life span, reduced body weight, and bone and cardiovascular abnormalities. The cardiovascular phenotype evident in the $Lmna^{G609G}$ mice resembles that of HGPS patients, as assessed by the loss of VSMCs and the alterations in ECG parameters. These similarities are a unique feature of this animal model when compared with previously available models of HGPS (*38*) and may facilitate further studies about the role of A-type lamins in cardiovascular pathophysiology during normal and pathological aging.

In addition, $Lmna^{G609G}$ knock-in mice may help to clarify the relevance of systemic factors as regulators of aging. Recent work has pinpointed metabolic alterations in several mouse progeria models (*15*, *21*, *27*, *39*). Accordingly, $Lmna^{G609G/G609G}$ animals also exhibited changes in several metabolic parameters, including blood insulin, leptin, and adiponectin concentrations, which are probably related to the altered glucose and lipid metabolism displayed by these mice. Likewise, $Lmna^{G609G/G609G}$ showed a marked dysregulation of the somatotroph axis, with a reduction and increase in blood levels of IGF-1 and GH, respectively, a situation that resembles a GH resistance condition known as Laron syndrome (*40*, *41*).

We have also demonstrated in this work that the combined administration of two antisense oligonucleotides that block the aberrant splicing in *Lmna* caused by the c.1827C>T;p.Gly609Gly mutation reduces progerin amounts in vivo. The fact that we could not observe a significant reduction of progerin levels in skeletal muscle could be the result of lower vivo-morpholino uptake in this tissue compared with liver or kidney, in which progerin expression was markedly downregulated. Notably, we have also shown that progerin reduction mediated by vivo-morpholino treatment significantly expands the life expectancy of $Lmna^{G609G/G609G}$ mice and ameliorates most phenotypical and molecular alterations in these animals relative to untreated mice, including a significant reduction in the expression of p53 target genes and a normalization of blood glucose levels.

Together, these findings provide an in vivo demonstration of the feasibility of ameliorating the characteristic alterations caused by progerin-linked premature aging through splicing modulation. Our results also suggest that these reagents might be tested in a future clinical trial for the treatment of HGPS. Setting up of therapeutic trials for rare diseases such as progeroid syndromes (*38*, *42*) is extremely challenging because of the lack of extensive clinical longitudinal studies with homogeneous evaluation parameters on cohorts of patients, which hinders the definition of homogeneous therapeutic outcome measures and endpoints. Also, multicentric trials are difficult to organize because of the very low number of patients within a single country, which hampers the strict application of identical protocols in various participating clinical investigation centers.

These difficulties have often prevented translation from established therapeutic proofs of principle to phase 1 and 2 clinical trials. However, the ongoing clinical trials in HGPS patients mentioned above have demonstrated the feasibility of designing and conducting a therapeutic trial for progeria and may serve as a basis for the design of a novel protocol that tests the oligonucleotides used in the present study. Furthermore, the development of this splicing-directed protocol for HGPS treatment may be facilitated by antisense oligonucleotide–based therapies that have already displayed preclinical efficacy in several other diseases (*43*) and are being currently tested in clinical trials for Duchenne muscular dystrophy (*44*).

## MATERIALS AND METHODS

### Gene targeting of *Lmna* gene

DNA fragments for the arms of the gene-targeting vector were generated by PCR of genomic DNA from 129/Ola embryonic stem (ES) cells. A 4.4-kb 5′-homology arm, spanning from exon 3 to the middle of exon 10, was amplified and cloned in the 5′-polylinker of a modified PGKNeotpalox2 vector into which we had previously introduced the *thymidine kinase* selection gene. Next, we cloned the 5.6-kb 3′-homology arm, which spanned from exon 10 to the end of the gene, in the 3′-polylinker of PGKNeotpalox2. To this end, we amplified and cloned two subfragments. The first one, which spanned to the end of exon 11, was amplified with a reverse oligonucleotide that contained the c.1827C>T mutation. Vector integrity was verified by DNA sequencing and restriction mapping. The targeting vector was linearized and electroporated into strain 129/Ola ES cells. To identify clones that carried the targeted $Lmna^{LCS}$ allele, we performed Southern (DNA) blot analysis of Hind III– and Bsp HI–digested genomic DNA. The probes detected 9.8- and 10.5-kb fragments, respectively, in the recombinant allele. Mouse genotyping was performed by PCR of genomic DNA with the following oligonucleotides: 5′-AAGGGGCTGGGAGGACAGAG-3′, 5′-AGTAGAAGGTGGCGCGAAGG-3′, and 5′-AGCATGCAATAGGGTGGAAGGA-3′. The PCR fragment consisted of 340 base pairs (bp) from the $Lmna^{LCS}$ allele and 100 bp from the wild-type allele. Targeted 129/Ola ES cells were microinjected into C57BL/6 mouse blastocysts to produce chimeric mice that were then crossed with C57BL/6 mice to generate heterozygous $Lmna^{LCS}$ mice. Electroporation of the targeting vector and microinjection of ES cells were performed in the facilities available at Centre D'Immunologie de Marseille-Luminy (Marseille-Luminy, France) under the supervision of B. Malissen. To generate mice that carry the $Lmna^{G609G}$ allele, we crossed $Lmna^{LCS}$ mice with transgenic mice that express constitutive cytomegalovirus Cre recombinase (Jackson Laboratory), and we verified cassette excision by PCR. The nomenclature for the description of sequence variants follows the Human Genome Variation Society guidelines given at http://www.hgvs.org/mutnomen/. The reference sequences used for

sequence variation description were as follows: human *LMNA* NM_170707.2 and mouse *Lmna* NM_001002011.2.

### Animal experiments

We performed animal experiments in accordance with the guidelines of the Committee for Animal Experimentation of the Universidad de Oviedo and the Regional Ethics Committee for Animal Experimentation (Provence Committee). μCT analyses of bones were performed with a μCT Skyscan 1172 system (Skyscan). Forepaw strength of $Lmna^{G609G/G609G}$, $Lmna^{G609G/+}$, and $Lmna^{+/+}$ male mice was measured with a strain gauge sensor (Bioseb). We administrated combined vivo-morpholinos (Gene Tools, LLC) MmEx10-MmEx11 at a concentration of 6 mg/kg each in phosphate-buffered saline (PBS) through tail vein injection twice per week. Control vivo-morpholino was administrated according to the same routine at a concentration of 12 mg/kg in PBS. Mice were treated for 12 weeks, starting at the age of 6 weeks. Treatment with vehicle alone or control vivo-morpholinos did not produce any apparent damage or stress in control mice. For histology analysis, we fixed samples with 4% paraformaldehyde in PBS, processed the resulting preparations into serial paraffin sections, and stained each with either 4′,6-diamidino-2-phenylindole (DAPI) or hematoxylin and eosin (H&E).

### Genomic and transcriptional characterization

DNA was extracted from mouse tails following standard procedures. Genotyping was performed with the following primers: DNA-Mm-Lmna forward, 5′-GGTTCCCACTGCAGCGGCTC-3′ (exon 11), and DNA-Mm-Lmna reverse, 5′-GGACCCCACTCCCTTGGGCT-3′ (intron 11). Direct sequencing was performed with an ABI Prism 3130XL automatic sequencer (Applied Biosystems). Total RNA was extracted with PureLink RNA Mini Kit (Invitrogen) and treated with deoxyribonuclease (Invitrogen). Total RNA (500 ng) was retrotranscribed with the high-capacity reverse transcription kit (Applied Biosystems). PCR primers that encompassed exon 11 were used for both amplification and sequencing: Mm-Lmna 10 forward, 5′-AGAGCTCCTCCATCACCACCGT-3′, and Mm-Lmna 12 reverse, 5′-TGCCTGGCAGGTCCCAGATT-3′.

### Morpholino sequences

The morpholino oligonucleotides used in this study were as follows: MmEx10 (5′-GCTGCCACTCACACGGTGGTGATGG-3′), MmEx11 (5′-GGATCCACCCACCTGGGCTCCCGCT-3′), and a negative control (5′-CCTCTTACCTCAGTTACAATTTATA-3′) for mouse cells and in vivo experiments, and HsEx10 (5′-GCTACCACTCACGTGGTGGTGATGG-3′) and HsEx11 (5′-GGGTCCACCCACCTGGGCTCCTGAG-3′) for human cell experiments (Gene Tools, LLC).

### Cell culture

We extracted mouse fibroblasts from 8-week-old ears as previously described (*32*). Human skin fibroblasts from control subjects (AG10803) and patients who carried the HGPS p.Gly608Gly mutation (AG01972c) were obtained from the Coriell Cell Repository. We maintained all cultures in Dulbecco's modified Eagle's medium (Gibco) supplemented with 10% fetal bovine serum (Gibco) and 1% antibiotic-antimycotic (Gibco). For transfection of the morpholinos, we followed the manufacturer's instructions (Gene Tools, LLC). Briefly, cells were plated at a high density (80%), and varying amounts of each morpholino were added to the cell cultures. Next, we added *endoporter* reagent at a final concentration of 6 μM (Gene Tools, LLC). Cells were retransfected 48 hours later following the same routine. Western (immuno) blot and inmunofluorescence analyses were performed 96 hours after the first transfection of the morpholinos. Analyses in primary mouse fibroblasts were performed at P5 and in HGPS human fibroblasts at passage 16.

### Western (immuno) blot analysis

Cultured cells were washed twice with 1× PBS and resuspended in 2× Laemmli buffer. Tissues were snap-frozen in liquid nitrogen. Frozen tissues (~50 mg in each sample) were homogenized in 300 μl of 100 mM tris-HCl (pH 7.4), 2% SDS, and 50 mM EDTA with a Polytron homogenizer. Protein concentration was evaluated with the bicinchoninic acid technique (Pierce BCA Protein Assay Kit). Equal amounts of proteins were loaded onto 8% SDS-polyacrylamide gels. After electrophoresis, gels were electrotransferred onto nitrocellulose membranes or Immobilon-FL polyvinylidene fluoride membranes (Millipore), blocked with 5% nonfat dry milk in TBS-T buffer [20 mM tris (pH 7.4), 150 mM NaCl, and 0.05% Tween 20] or in Odyssey Blocking Buffer diluted 1:1 in PBS for 1 hour at room temperature, and incubated overnight at 4°C or 1 hour at room temperature with various primary antibodies: 1:500 monoclonal anti–lamin A/C (Manlac-1, provided by G. Morris), 1:1000 goat polyclonal anti–lamin A/C (sc-20681 and sc-6215, Santa Cruz Biotechnology), 1:40,000 monoclonal anti–glyceraldehyde-3-phosphate dehydrogenase (GAPDH) (MAB374, Millipore), 1:10,000 anti–α-tubulin (T6074, Sigma), or 1:10,000 anti–β-actin (AC-40, Sigma). Finally, blots were incubated with 1:10,000 goat anti-mouse horseradish peroxidase (HRP) (Jackson ImmunoResearch Laboratories) in 1.5% nonfat milk in TBS-T or 1:15,000 IR-Dye 800–conjugated secondary donkey anti-goat and anti-mouse antibodies in Odyssey blocking buffer. Then, we washed and developed the immunoreactive bands with Immobilon Western chemiluminescent HRP substrate (Millipore). For IR-Dye 800 detection, an Odyssey Infrared Imaging System (LI-COR Biosciences) was used.

### Immunofluorescence analysis

Cells were fixed in 4% paraformaldehyde solution, rinsed in PBS, and permeabilized with 0.5% Triton X-100. A different permeabilization step was needed for γH2AX staining, which was performed with a 0.1% sodium citrate and 0.1% Triton X-100 solution. The antibodies used were anti–lamin A/C (Manlac-1, 1:50) or anti-γH2AX (Millipore, 1:300). Cells were incubated with primary antibodies diluted in PBS (supplemented with 1% bovine serum albumin) for 1 to 3 hours at 25°C. After washes with PBS, slides were incubated with 1:100 rhodamine-conjugated donkey anti-mouse secondary antibody (Jackson ImmunoResearch Laboratories) for 1 hour at 25°C. After the final washes, nuclei were counterstained with DAPI (Roche), and slides were mounted in Vectashield mounting medium (Vector). Microphotographs were recorded with an Axioplan-2 Zeiss fluorescent microscope (Zeiss), and images were captured with a charge-coupled device camera (Photometrics SenSys). The nuclei of progeroid and normal fibroblasts were then counted ($n$ = 300 for each experiment).

### RNA preparation and quantitative RT-PCR

Collected tissue was immediately homogenized in TRIzol reagent (Invitrogen) and processed through alcohol precipitation. RNA pellets were then washed in cold 75% ethanol and resuspended in nuclease-free water (Ambion), and the samples were quantified and evaluated

for purity (260-nm/280-nm ratio) with a NanoDrop ND-1000 spectrophotometer. cDNA was synthesized with 1 to 4 μg of total RNA with the ThermoScript RT-PCR system (Invitrogen). For detection of aberrant splicing of the *Lmna* gene, the following oligonucleotides were used: Lmna-9F (5′-GTGGAAGGCGCAGAACACCT-3′) and Lmna-12R (5′-GTGAGGGGGGAGCAGGTG-3′). The oligonucleotides used for specific amplification of the lamin C–encoding mRNA transcript were Lmna-7F (5′-CCAGCCCTACCTCGCAGC-3′) and Lmna-10R (5′-GCGGCGGCTGCCACTCAC-3′) (*23*). Mouse *Gapdh* mRNA was used as an endogenous control, and the corresponding cDNA was amplified with the following primers: Gapdh-F (5′-GTGCAGTGCCAGCCTCGTCC-3′) and Gapdh-R (5′-GCCACTGCAAATGGCAGCCC-3′). Quantitative RT-PCR (qRT-PCR) was carried out in triplicate for each sample with 20 ng of cDNA, TaqMan Universal PCR Master Mix, and 1 μl of the specific TaqMan custom gene expression assay solution for the gene of interest (Applied Biosystems). For the mouse progerin qRT-PCR experiments, the following oligonucleotides and probe were used: MmProgerin_fwd (5′-TGAGTACAACCTGCGCTCAC-3′), MmProgerin_rev (5′-TGGCAGGTCCCAGATTACAT-3′), and MmProgerin_probe (5′-CGGGAGCCCAGAGCTCCCAGAA-3′). As an internal control for the amount of template cDNA used, gene expression was normalized to amounts obtained for the mouse *Gapdh* endogenous control.

### Heart analysis and blood pressure

We anesthetized mice with 2.5% sevoflurane and used a Vevo 2100 transthoracic echocardiograph equipped with a 30-MHz mouse ultrasound probe to assess left ventricular function and ECG parameters (PR and QRS intervals) with the VevoStrain software (Visual Sonic). Blood pressure and heart rate were measured with a noninvasive automated tail-cuff device (Visitech System BP2000). Mice were trained on a daily basis for 1 week, and then measurements were taken on a weekly basis at the same time in the morning. For more accuracy, the first 10 of 20 measurements were discarded, and mean values of the last 10 measurements for individual mice were used for analysis.

### Blood and plasma parameters

Animals were starved for 6 hours before measurement to avoid any possible alteration in blood glucose concentrations as a result of food intake. Blood glucose was measured with an Accu-Chek glucometer (Roche Diagnostics) using blood from the tail vein. For other measured parameters, blood was extracted directly from the mandibular sinus after anesthetizing mice with isoflurane. To obtain plasma, we centrifuged blood immediately after collection at 3000*g* at 4°C, and we collected the supernatant and stored it at −20°C until analysis. Plasma IGF-1 concentrations were determined with the Quantikine ELISA (enzyme-linked immunosorbent assay) kit (R&D Systems), whereas plasma GH concentrations were measured with the Linco ELISA kit. For plasma insulin, leptin, and adiponectin measurements, we used Millipore ELISA Kits. All protocols were performed according to the manufacturer's instructions.

### Transcriptional profiling

Total RNA was isolated with an RNeasy kit (Qiagen). Double-stranded cDNA was synthesized with the SuperScript cDNA synthesis kit (Invitrogen). In vitro transcription was carried out with the Bioarray high-yield RNA transcript labeling kit (Enzo Diagnostics). The biotin-labeled complementary RNA (cRNA) was purified, fragmented, and hybridized to a GeneChip Mouse Gene 1.0 ST Array (Affymetrix). Washing and scanning were performed with a Fluidics Station 400 and GeneChip Scanner (Affymetrix). After scanning, raw data were processed with the RMAExpress program (http://RMAExpress.bmbolstad.com) using default settings.

### Gene set enrichment analysis

GSEA was performed as described in the original citation (*31*). For data analysis, we used GSEA release 2.06 and MSigDB release 2.5 (http://www.broadinstitute.org/gsea/index.jsp). Weighted enrichment scores were calculated with gene expression lists ranked by signal-to-noise ratio. The maximum gene set size was set to 500 genes; the minimum gene set size was set to 20 genes; the number of permutations was set to 1000. Analyses were performed with a collection of gene sets from curated genes and canonical pathways. Selected enriched pathways had a relaxed false discovery rate of $\leq 0.25$ and $P \leq 0.01$.

### Statistical analysis

We performed statistical analysis of the differences between mouse cohorts or treated and untreated cells with a two-tailed Student's *t* test. In experiments with more than two groups, differences were analyzed by multifactorial one-way analysis of variance (ANOVA). We performed statistical analysis on the differences between positive nuclei in indirect immunofluorescence experiments with ANOVA and Cohen's *d* Ryan test. The analysis of covariance (ANCOVA) with the body mass as the covariate was used to analyze the grip strength test results. We used Microsoft Excel or GraphPad Prism software for calculations and expressed the results as the means ± SDs.

## SUPPLEMENTARY MATERIAL

www.sciencetranslationalmedicine.org/cgi/content/full/3/106/106ra107/DC1

Fig. S1. Genomic sequencing of *Lmna* exon 11 in $Lmna^{+/+}$, $Lmna^{G609G/+}$, and $Lmna^{G609G/G609G}$ mice.

Fig. S2. Western (immuno) blot analysis of human control fibroblasts (AG10803), human HGPS fibroblasts (AG01972c), and tissues from $Lmna^{+/+}$, $Lmna^{G609G/+}$, and $Lmna^{G609G/G609G}$ mice.

Fig. S3. Phenotypic characterization of $Lmna^{LCS/LCS}$ mice.

Fig. S4. Organ size evaluation in 3-month-old $Lmna^{G609G/G609G}$ versus $Lmna^{+/+}$ mice.

Fig. S5. μCT analysis of bone alterations in $Lmna^{G609G/G609G}$ mice.

Fig. S6. Cardiovascular phenotype of $Lmna^{G609G/G609G}$ mice.

Fig. S7. Enrichment score plots from GSEA-extracted representative pathways containing genes enriched in $Lmna^{G609G/G609G}$ mice samples.

Fig. S8. Enrichment score plots of GSEA-extracted representative pathways containing genes enriched in $Lmna^{+/+}$ mice samples.

Fig. S9. Nuclear envelope architecture analyzed in an HGPS fibroblast cell line (AG01972c) treated with HsEx10 and HsEx11 morpholinos.

Fig. S10. RT-PCR analysis in tissues from $Lmna^{+/+}$, untreated $Lmna^{G609G/G609G}$, and MmEx10-11–treated $Lmna^{G609G/G609G}$ and $Lmna^{G609G/+}$ mice.

Fig. S11. Western (immuno) blot analysis of lamin A/C in tissues from treated and untreated $Lmna^{G609G/G609G}$ mice.

Fig. S12. Phenotypic characterization of MmEx10-11–treated $Lmna^{G609G/G609G}$ mice.

Table S1. Affymetrix Mouse Gene 1.0 ST probes showing the greatest increase or decrease ($P < 0.005$) in liver from $Lmna^{G609G/G609G}$ mutant mice.

## REFERENCES AND NOTES

1. R. C. Hennekam, Hutchinson–Gilford progeria syndrome: Review of the phenotype. *Am. J. Med. Genet. A* **140**, 2603–2624 (2006).
2. M. A. Merideth, L. B. Gordon, S. Clauss, V. Sachdev, A. C. Smith, M. B. Perry, C. C. Brewer, C. Zalewski, H. J. Kim, B. Solomon, B. P. Brooks, L. H. Gerber, M. L. Turner, D. L. Domingo, T. C. Hart, J. Graf, J. C. Reynolds, A. Gropman, J. A. Yanovski, M. Gerhard-Herman, F. S. Collins, E. G. Nabel, R. O. Cannon III, W. A. Gahl, W. J. Introne, Phenotype and course of Hutchinson–Gilford progeria syndrome. *N. Engl. J. Med.* **358**, 592–604 (2008).

3. A. De Sandre-Giovannoli, R. Bernard, P. Cau, C. Navarro, J. Amiel, I. Boccaccio, S. Lyonnet, C. L. Stewart, A. Munnich, M. Le Merrer, N. Lévy, Lamin a truncation in Hutchinson-Gilford progeria. *Science* **300**, 2055 (2003).
4. M. Eriksson, W. T. Brown, L. B. Gordon, M. W. Glynn, J. Singer, L. Scott, M. R. Erdos, C. M. Robbins, T. Y. Moses, P. Berglund, A. Dutra, E. Pak, S. Durkin, A. B. Csoka, M. Boehnke, T. W. Glover, F. S. Collins, Recurrent de novo point mutations in lamin A cause Hutchinson–Gilford progeria syndrome. *Nature* **423**, 293–298 (2003).
5. H. J. Worman, R. Foisner, The nuclear envelope from basic biology to therapy. *Biochem. Soc. Trans.* **38**, 253–256 (2010).
6. Y. Gruenbaum, A. Margalit, R. D. Goldman, D. K. Shumaker, K. L. Wilson, The nuclear lamina comes of age. *Nat. Rev. Mol. Cell Biol.* **6**, 21–31 (2005).
7. P. Scaffidi, T. Misteli, Lamin A-dependent nuclear defects in human aging. *Science* **312**, 1059–1063 (2006).
8. C. R. Burtner, B. K. Kennedy, Progeria syndromes and ageing: What is the connection? *Nat. Rev. Mol. Cell Biol.* **11**, 567–578 (2010).
9. A. M. Pendás, Z. Zhou, J. Cadiñanos, J. M. Freije, J. Wang, K. Hultenby, A. Astudillo, A. Wernerson, F. Rodríguez, K. Tryggvason, C. López-Otín, Defective prelamin A processing and muscular and adipocyte alterations in Zmpste24 metalloproteinase–deficient mice. *Nat. Genet.* **31**, 94–99 (2002).
10. M. O. Bergo, B. Gavino, J. Ross, W. K. Schmidt, C. Hong, L. V. Kendall, A. Mohr, M. Meta, H. Genant, Y. Jiang, E. R. Wisner, N. Van Bruggen, R. A. Carano, S. Michaelis, S. M. Griffey, S. G. Young, *Zmpste24* deficiency in mice causes spontaneous bone fractures, muscle weakness, and a prelamin A processing defect. *Proc. Natl. Acad. Sci. U.S.A.* **99**, 13049–13054 (2002).
11. S. H. Yang, M. O. Bergo, J. I. Toth, X. Qiao, Y. Hu, S. Sandoval, M. Meta, P. Bendale, M. H. Gelb, S. G. Young, L. G. Fong, Blocking protein farnesyltransferase improves nuclear blebbing in mouse fibroblasts with a targeted Hutchinson–Gilford progeria syndrome mutation. *Proc. Natl. Acad. Sci. U.S.A.* **102**, 10291–10296 (2005).
12. R. Varga, M. Eriksson, M. R. Erdos, M. Olive, I. Harten, F. Kolodgie, B. C. Capell, J. Cheng, D. Faddah, S. Perkins, H. Avallone, H. San, X. Qu, S. Ganesh, L. B. Gordon, R. Virmani, T. N. Wight, E. G. Nabel, F. S. Collins, Progressive vascular smooth muscle cell defects in a mouse model of Hutchinson–Gilford progeria syndrome. *Proc. Natl. Acad. Sci. U.S.A.* **103**, 3250–3255 (2006).
13. Y. Wang, A. A. Panteleyev, D. M. Owens, K. Djabali, C. L. Stewart, H. J. Worman, Epidermal expression of the truncated prelamin A causing Hutchinson–Gilford progeria syndrome: Effects on keratinocytes, hair and skin. *Hum. Mol. Genet.* **17**, 2357–2369 (2008).
14. H. Sagelius, Y. Rosengardten, M. Hanif, M. R. Erdos, B. Rozell, F. S. Collins, M. Eriksson, Targeted transgenic expression of the mutation causing Hutchinson–Gilford progeria syndrome leads to proliferative and degenerative epidermal disease. *J. Cell Sci.* **121**, 969–978 (2008).
15. G. Mariño, A. P. Ugalde, N. Salvador-Montoliu, I. Varela, P. M. Quirós, J. Cadiñanos, I. van der Pluijm, J. M. Freije, C. López-Otín, Premature aging in mice activates a systemic metabolic response involving autophagy induction. *Hum. Mol. Genet.* **17**, 2196–2211 (2008).
16. J. Espada, I. Varela, I. Flores, A. P. Ugalde, J. Cadiñanos, A. M. Pendás, C. L. Stewart, K. Tryggvason, M. A. Blasco, J. M. Freije, C. López-Otín, Nuclear envelope defects cause stem cell dysfunction in premature-aging mice. *J. Cell Biol.* **181**, 27–35 (2008).
17. H. J. Worman, L. G. Fong, A. Muchir, S. G. Young, Laminopathies and the long strange trip from basic cell biology to therapy. *J. Clin. Invest.* **119**, 1825–1836 (2009).
18. F. G. Osorio, I. Varela, E. Lara, X. S. Puente, J. Espada, R. Santoro, J. M. Freije, M. F. Fraga, C. López-Otín, Nuclear envelope alterations generate an aging-like epigenetic pattern in mice deficient in Zmpste24 metalloprotease. *Aging Cell* **9**, 947–957 (2010).
19. S. H. Yang, M. Meta, X. Qiao, D. Frost, J. Bauch, C. Coffinier, S. Majumdar, M. O. Bergo, S. G. Young, L. G. Fong, A farnesyltransferase inhibitor improves disease phenotypes in mice with a Hutchinson-Gilford progeria syndrome mutation. *J. Clin. Invest.* **116**, 2115–2121 (2006).
20. I. Varela, S. Pereira, A. P. Ugalde, C. L. Navarro, M. F. Suárez, P. Cau, J. Cadiñanos, F. G. Osorio, N. Foray, J. Cobo, F. de Carlos, N. Lévy, J. M. Freije, C. López-Otín, Combined treatment with statins and aminobisphosphonates extends longevity in a mouse model of human premature aging. *Nat. Med.* **14**, 767–772 (2008).
21. G. Mariño, A. P. Ugalde, A. F. Fernández, F. G. Osorio, A. Fueyo, J. M. Freije, C. López-Otín, Insulin-like growth factor 1 treatment extends longevity in a mouse model of human premature aging by restoring somatotroph axis function. *Proc. Natl. Acad. Sci. U.S.A.* **107**, 16268–16273 (2010).
22. K. Cao, J. J. Graziotto, C. D. Blair, J. R. Mazzulli, M. R. Erdos, D. Krainc, F. S. Collins, Rapamycin reverses cellular phenotypes and enhances mutant protein clearance in Hutchinson-Gilford progeria syndrome cells. *Sci. Transl. Med.* **3**, 89ra58 (2011).
23. P. Scaffidi, T. Misteli, Reversal of the cellular phenotype in the premature aging disease Hutchinson-Gilford progeria syndrome. *Nat. Med.* **11**, 440–445 (2005).
24. L. G. Fong, J. K. Ng, J. Lammerding, T. A. Vickers, M. Meta, N. Coté, B. Gavino, X. Qiao, S. Y. Chang, S. R. Young, S. H. Yang, C. L. Stewart, R. T. Lee, C. F. Bennett, M. O. Bergo, S. G. Young, Prelamin A and lamin A appear to be dispensable in the nuclear lamina. *J. Clin. Invest.* **116**, 743–752 (2006).
25. C. L. Navarro, J. Cadiñanos, A. De Sandre-Giovannoli, R. Bernard, S. Courrier, I. Boccaccio, A. Boyer, W. J. Kleijer, A. Wagner, F. Giuliano, F. A. Beemer, J. M. Freije, P. Cau, R. C. Hennekam, C. López-Otín, C. Badens, N. Lévy, Loss of ZMPSTE24 (FACE-1) causes autosomal recessive restrictive dermopathy and accumulation of lamin A precursors. *Hum. Mol. Genet.* **14**, 1503–1513 (2005).
26. J. S. Hale, R. L. Frock, S. A. Mamman, P. J. Fink, B. K. Kennedy, Cell-extrinsic defective lymphocyte development in *Lmna*$^{-/-}$ mice. *PLoS One* **5**, e10127 (2010).
27. R. Mostoslavsky, K. F. Chua, D. B. Lombard, W. W. Pang, M. R. Fischer, L. Gellon, P. Liu, G. Mostoslavsky, S. Franco, M. M. Murphy, K. D. Mills, P. Patel, J. T. Hsu, A. L. Hong, E. Ford, H. L. Cheng, C. Kennedy, N. Nunez, R. Bronson, D. Frendewey, W. Auerbach, D. Valenzuela, M. Karow, M. O. Hottiger, S. Hursting, J. C. Barrett, L. Guarente, R. Mulligan, B. Demple, G. D. Yancopoulos, F. W. Alt, Genomic instability and aging-like phenotype in the absence of mammalian SIRT6. *Cell* **124**, 315–329 (2006).
28. M. Olive, I. Harten, R. Mitchell, J. K. Beers, K. Djabali, K. Cao, M. R. Erdos, C. Blair, B. Funke, L. Smoot, M. Gerhard-Herman, J. T. Machan, R. Kutys, R. Virmani, F. S. Collins, T. N. Wight, E. G. Nabel, L. B. Gordon, Cardiovascular pathology in Hutchinson-Gilford progeria: Correlation with the vascular pathology of aging. *Arterioscler. Thromb. Vasc. Biol.* **30**, 2301–2309 (2010).
29. W. E. Stehbens, B. Delahunt, T. Shozawa, E. Gilbert-Barness, Smooth muscle cell depletion and collagen types in progeric arteries. *Cardiovasc. Pathol.* **10**, 133–136 (2001).
30. T. Dechat, K. Pfleghaar, K. Sengupta, T. Shimi, D. K. Shumaker, L. Solimando, R. D. Goldman, Nuclear lamins: Major factors in the structural organization and function of the nucleus and chromatin. *Genes Dev.* **22**, 832–853 (2008).
31. A. Subramanian, P. Tamayo, V. K. Mootha, S. Mukherjee, B. L. Ebert, M. A. Gillette, A. Paulovich, S. L. Pomeroy, T. R. Golub, E. S. Lander, J. P. Mesirov, Gene set enrichment analysis: A knowledge-based approach for interpreting genome-wide expression profiles. *Proc. Natl. Acad. Sci. U.S.A.* **102**, 15545–15550 (2005).
32. I. Varela, J. Cadiñanos, A. M. Pendás, A. Gutiérrez-Fernández, A. R. Folgueras, L. M. Sánchez, Z. Zhou, F. J. Rodríguez, C. L. Stewart, J. A. Vega, K. Tryggvason, J. M. Freije, C. López-Otín, Accelerated ageing in mice deficient in Zmpste24 protease is linked to p53 signalling activation. *Nature* **437**, 564–568 (2005).
33. B. Liu, J. Wang, K. M. Chan, W. M. Tjia, W. Deng, X. Guan, J. D. Huang, K. M. Li, P. Y. Chau, D. J. Chen, D. Pei, A. M. Pendas, J. Cadiñanos, C. López-Otín, H. F. Tse, C. Hutchison, J. Chen, Y. Cao, K. S. Cheah, K. Tryggvason, Z. Zhou, Genomic instability in laminopathy-based premature aging. *Nat. Med.* **11**, 780–785 (2005).
34. L. Zhong, A. D'Urso, D. Toiber, C. Sebastian, R. E. Henry, D. D. Vadysirisack, A. Guimaraes, B. Marinelli, J. D. Wikstrom, T. Nir, C. B. Clish, B. Vaitheesvaran, O. Iliopoulos, I. Kurland, Y. Dor, R. Weissleder, O. S. Shirihai, L. W. Ellisen, J. M. Espinosa, R. Mostoslavsky, The histone deacetylase Sirt6 regulates glucose homeostasis via Hif1α. *Cell* **140**, 280–293 (2010).
35. J. Summerton, Morpholino antisense oligomers: The case for an RNase H-independent structural type. *Biochim. Biophys. Acta* **1489**, 141–158 (1999).
36. M. K. Parra, S. Gee, N. Mohandas, J. G. Conboy, Efficient in vivo manipulation of alternative pre-mRNA splicing events using antisense morpholinos in mice. *J. Biol. Chem.* **286**, 6033–6039 (2011).
37. P. A. Morcos, Y. Li, S. Jiang, Vivo-Morpholinos: A non-peptide transporter delivers Morpholinos into a wide array of mouse tissues. *Biotechniques* **45**, 613–614 (2008).
38. F. G. Osorio, A. J. Obaya, C. López-Otín, J. M. Freije, Accelerated ageing: From mechanism to therapy through animal models. *Transgenic Res.* **18**, 7–15 (2009).
39. L. J. Niedernhofer, G. A. Garinis, A. Raams, A. S. Lalai, A. R. Robinson, E. Appeldoorn, H. Odijk, R. Oostendorp, A. Ahmad, W. van Leeuwen, A. F. Theil, W. Vermeulen, G. T. van der Horst, P. Meinecke, W. J. Kleijer, J. Vijg, N. G. Jaspers, J. H. Hoeijmakers, A new progeroid syndrome reveals that genotoxic stress suppresses the somatotroph axis. *Nature* **444**, 1038–1043 (2006).
40. Z. Laron, Laron syndrome (primary growth hormone resistance or insensitivity): The personal experience 1958–2003. *J. Clin. Endocrinol. Metab.* **89**, 1031–1044 (2004).
41. A. P. Ugalde, G. Mariño, C. López-Otín, Rejuvenating somatotropic signaling: A therapeutical opportunity for premature aging? *Aging* **2**, 1017–1022 (2010).
42. X. S. Puente, V. Quesada, F. G. Osorio, R. Cabanillas, J. Cadiñanos, J. M. Fraile, G. R. Ordóñez, D. A. Puente, A. Gutiérrez-Fernández, M. Fanjul-Fernández, N. Lévy, J. M. Freije, C. López-Otín, Exome sequencing and functional analysis identifies *BANF1* mutation as the cause of a hereditary progeroid syndrome. *Am. J. Hum. Genet.* **88**, 650–656 (2011).
43. S. M. Hammond, M. J. Wood, Genetic therapies for RNA mis-splicing diseases. *Trends Genet.* **27**, 196–205 (2011).
44. S. Cirak, V. Arechavala-Gomeza, M. Guglieri, L. Feng, S. Torelli, K. Anthony, S. Abbs, M. E. Garralda, J. Bourke, D. J. Wells, G. Dickson, M. J. Wood, S. D. Wilton, V. Straub, R. Kole, S. B. Shrewsbury, C. Sewry, J. E. Morgan, K. Bushby, F. Muntoni, Exon skipping and dystrophin restoration in patients with Duchenne muscular dystrophy after systemic phosphorodiamidate morpholino oligomer treatment: An open-label, phase 2, dose-escalation study. *Lancet* **378**, 595–605 (2011).

45. **Acknowledgments:** We thank G. Velasco, A. Fueyo, A. Ramsay, J. Valcárcel, M. S. Fernández, P. Roubertoux, M. G. Mattei, C. Tardieu, P. Cau, P. Roll, M. J. Andrés-Manzano, J. M. González, B. Malissen, and L. J. Jiménez-Borreguero for their support and assistance. **Funding:** This work was supported by grants from Ministerio de Ciencia e Innovación-Spain, PCTI-FICYT Asturias, European Union (FP7 MicroEnviMet), Botín Foundation, Red de Investigación en Enfermedades Cardiovasculares (RECAVA), Institut National de la Santé et de la Recherche Médicale, Agence Nationale de la Recherche, and Association Française contre les Myopathies. The Instituto Universitario de Oncología is supported by Obra Social Cajastur and Acción Transversal del Cáncer-Red Temática de Investigación Cooperativa en Cáncer (RTICC). **Author contributions:** F.G.O., C.L.N., I.C.L.-M., C.B., A.D.S.-G., and J.T. carried out animal experiments. J. Cadiñanos and J.M.P.F. designed and generated the targeting vector. F.G.O., P.M.Q., I.V., C.L.N., and D.D. performed molecular biology and cell culture–based studies. J.R., G.G., and V.A. carried out cardiovascular analyses. F.d.C. and J. Cobo conducted μCT analysis. C.L.-O., J.M.P.F., and N.L. were responsible for designing and supervising the project. C.L.-O., F.G.O., J.M.P.F., and N.L. wrote the manuscript. **Competing interests:** The authors declare that they have no competing interests. **Accession numbers:** RNA expression data are available at the Gene Expression Omnibus repository (accession number GSE32609).

Submitted 30 June 2011
Accepted 20 September 2011
Published 26 October 2011
10.1126/scitranslmed.3002847

**Citation:** F. G. Osorio, C. L. Navarro, J. Cadiñanos, I. C. López-Mejía, P. M. Quirós, C. Bartoli, J. Rivera, J. Tazi, G. Guzmán, I. Varela, D. Depetris, F. de Carlos, J. Cobo, V. Andrés, A. De Sandre-Giovannoli, J. M. P. Freije, N. Lévy, C. López-Otín, Splicing-directed therapy in a new mouse model of human accelerated aging. *Sci. Transl. Med.* **3**, 106ra107 (2011).